Role of nonadiabatic untrapped electrons in global electrostatic ion temperature gradient driven modes in a tokamak

J. Chowdhury,[1] R. Ganesh,[1,a)] P. Angelino,[2] J. Vaclavik,[3] L. Villard,[3] and S. Brunner[3]
[1]*Institute for Plasma Research, Bhat, Gandhinagar, India*
[2]*CEA/DSM/DRFC, Association Euratom-CEA, Cadarache, 13108 St. Paul-lez-Durance, France*
[3]*CRPP, Association EURATOM-Confédération Suisse, EPFL, 1015 Lausanne, Switzerland*

(Received 15 May 2008; accepted 23 June 2008; published online 25 July 2008)

In this work, role of nonadiabatic untrapped electrons in the context of a global ion temperature gradient driven mode has been investigated. In past studies, untrapped electrons have been assumed to be able to respond "instantaneously" to a disturbance. It is proposed that such adiabatic electron models should be reexamined for two important reasons: (i) It is known that global modes with n in the range of $3 \leqslant n \leqslant 15$ (n is the toroidal mode number) have eigenmode widths spanning several mode-rational surfaces. It is being argued that close to these mode-rational surfaces, adiabatic electron models fail and a consistent treatment of nonadiabatic electrons is crucial for global modes. (ii) Electromagnetic effects depend on passing nonadiabatic electron dynamics. A minimal nontrivial model for the benchmarking of global linear and nonlinear gyrokinetic codes in the future becomes necessary, which can treat both passing ions and electrons on the same physics footing. As a first step, a study of the effect of nonadiabatic passing electrons in global electrostatic ion temperature gradients is presented. Interesting results include a demonstration of multiscale structure, downshift in critical η_i with increasing η_e, and a reduction in mixing-length based transport. © *2008 American Institute of Physics*. [DOI: 10.1063/1.2957917]

I. INTRODUCTION

Tokamak plasmas, which are stable to ideal magnetohydrodynamic (MHD) disturbances, exhibit transport of particles and energy across confining magnetic flux surfaces. On longer time scales compared to particle and energy confinement times, such transport phenomena which arise due to equilibrium inhomogeneity are attributed to non-MHD-based low-frequency collisionless drift motion of particles.

Among others, toroidal ion temperature gradient driven drift modes (ITG),[1] trapped electron modes,[2] high-n Alfvén ion temperature gradient driven modes, or high-n kinetic ballooning modes[3] (n is the toroidal mode number) have been studied extensively both in linear and nonlinear regimes. For large n where it is expected that the mode structure would be localized to a magnetic flux surface, the ballooning formalism is a commonly used technique. For global modes with small n values, the usual ballooning formalism fails, thereby global linear and nonlinear gyrokinetic models become necessary.

For ITGs, such global gyrokinetic models show that the linear growth rate peaks between $n \simeq 3$ and 5 such that $k_\theta \rho_{\mathrm{Li}} \simeq 0.5$. For example, for typical DIII-D-like parameters, the global electrostatic toroidal gyrokinetic spectral model GLOGYSTO[4,5] and time-evolving gyrokinetic codes[6] report typical toroidal mode numbers in the range $3 \leqslant n \leqslant 15$ with eigenmode width and structure occupying a good fraction of the minor radius a. These eigenmodes span several mode rational surfaces (MRS) $r = r_{\mathrm{MRS}}$ defined as $k_{\parallel m,n}(r = r_{\mathrm{MRS}}) = 0$. In these models, the passing and trapped ions respond nonadiabatically while passing electrons are assumed adiabatic.

An electromagnetic version of GLOGYSTO called EM-GLOGYSTO has been developed by including passing drift kinetic electrons coupled to $A_\parallel$ fluctuations[7] followed by fully gyrokinetic electron dynamics coupled to $A_\parallel$ fluctuations and equilibrium flows.[8] The code EM-GLOGYSTO was generalized by including fully gyrokinetic nonadiabatic passing ion and electron dynamics which couple to $A_\perp$ fluctuations,[9] Shafranov shift effects,[10] followed by trapped electron dynamics coupled to $A_\perp$ fluctuations.[4,11] It has been shown that when passing drift kinetic electrons couple only to $A_\parallel$,[7] finite-β effects have a benign effect on ITGs with adiabatic electron response. Within the same model, Alfvén ITGs (AITGs) or kinetic ballooning modes (KBMs)[3,12–16] become more unstable with increasing β.[7,10] Subsequent studies[17] with the more accurate gyrokinetic nonadiabatic passing electron dynamics coupled to $A_\parallel$ fluctuations have shown about 10% change in growth rates of AITGs. However, in all the above-mentioned studies, the effect of nonadiabatic passing electrons when coupled to electrostatic fluctuations $\tilde{\phi}$ has not been explored.

In time-evolving gyrokinetic particle codes where ions are pushed by solving Newton's laws, the difference in mass ratio of ions and electrons imposes a stringent constraint on the numerical time-stepping. The assumption of adiabatic electron response simplifies the computational demands enormously. However, on a given magnetic flux surface, the adiabatic electron model is known to introduce spurious charge accumulation and zonal flows if electron adiabaticity is not carefully imposed.[18] For example, a widely used procedure in time-evolving gyrokinetic particle codes is to sub-

a)Electronic mail: ganesh@ipr.res.in.

tract a flux-surface averaged electrostatic fluctuation from the zonal component to enforce strict adiabaticity for electrons. If one were to push electrons with finite mass in a numerically consistent fashion, then such problems can be avoided. Because of the ion to electron mass ratio, the necessity of using small time steps is seen as a difficulty in time-evolving linear and nonlinear gyrokinetic particle codes. It goes without saying that the above-mentioned mass-ratio related physics issues are equally relevant to gyrokinetic Vlasov codes as well. For trapped electrons, more sophisticated models[19–21] are being developed, whereas for passing nonadiabatic electrons very few models exists. With more advanced physics models and larger computing facilities, nonadiabatic electron dynamics on the scale of tokamak minor radius and hence the global electrostatic and electromagnetic time-evolving simulations may become a reality.

Coming back to the global linear spectral models[4,7,10,17] described earlier, the above-mentioned difficulties found in time-evolving gyrokinetic linear/nonlinear codes are avoided as time evolution is replaced by frequency response of the system. As a result, at least for the linear regime, both ions and electrons can be handled on exactly the same physics footing. This situation provides a strong advantage in favor of the linear global gyrokinetic spectral models both physics-wise and also as a stringent numerical test case for future time-evolving nonlinear gyrokinetic codes with nonadiabatic electrons. To demonstrate the claim, we focus on global electrostatic ITGs with passing nonadiabatic ions, trapped ions, and passing nonadiabatic electrons. We bring out interesting qualitative and quantitative differences between ITGs with the usual adiabatic electron response compared with the nonadiabatic electrons response.

Such a study as presented here may be regarded as a minimal nontrivial model for the numerical benchmarking of present/future electrostatic global nonlinear gyrokinetic codes which would treat both ions and electrons on the same physics footing.

To this end, we focus on the electrostatic version of the fully gyrokinetic, fully electromagnetic global linear stability model EM-GLOGYSTO extensively studied and reported in Refs. 4, 7, 10, and 17 as applicable to large aspect ratio tokamaks. For the purposes of this study, Shafranov shift, equilibrium flows, trapped electron effects, $B_\perp$, and $B_\parallel$ fluctuations are dropped, while particle nonadiabaticity for passing ions, trapped ions, and passing electrons, Landau damping of passing species, finite Larmor radius (FLR) effects to all orders of all species, trapped and transit resonances, and poloidal and radial coupling of modes due to particle drifts across magnetic flux surfaces are included.

In Sec. II, starting from Vlasov equations, we outline the basic model solved, obtain our basic equation for the nonadiabatic part of the distribution function for a given passing species, introduce gyro-averaging and a solution for the passing particle nonadiabatic effect in "guiding center coordinates" in terms of a propagator, i.e., unit source solution, construction of the propagator, derive relevant fluctuations in "particle coordinates," closure using quasineutrality assumption, construction of various matrix elements in Fourier space, diagnostics, and normalizations. For other details of the EM model, the reader is referred to Refs. 9 and 10. Section III contains numerical results with adiabatic electrons as a benchmark and new results with nonadiabatic electrons followed by mode structure studies, mixing length based transport studies, η_e studies, and downshift of critical η_i are presented. Conclusions are presented in Sec. IV and some possible directions of future investigations are mentioned.

II. MODEL EQUATIONS

To describe hot toroidal plasmas, collisionless Vlasov–Maxwell equations are used. In the following, we invoke the standard technique of *gyrokinetic* change of variables as employed by Catto *et al.*[22] with an *eikonal or spectral ansatz* to obtain a gyrokinetic Vlasov equation. Among others, a self-consistent and energy-conserving theoretical framework was given by Hahm[23] based on Hamiltonian and Lie transformations, and more recently a variational formulation for the gyrokinetic Vlasov–Maxwell system was given by Brizard[24] resulting in gyrokinetic equations and gyro-averaged Maxwell's equations for finite-β plasmas. Theoretical formulations used here are an extension of those studied in Ref. 4 and 17 with a major change, namely the addition of the proper gyrokinetic nonadiabatic passing electron response to the electrostatic potential fluctuation. As our interest is in passing nonadiabatic electron dynamics, here we present a description of the electrostatic formulation. Readers interested in details of the EM formulation are referred to Ref. 9.

As appropriate for a linear stability study, the full distribution function $f_j(\mathbf{r},\mathbf{v},t)$ of species j is linearized about a suitable equilibrium $f_{0j}=f_{0j}(\mathbf{r},\mathbf{v})$ such that $f_j(\mathbf{r},\mathbf{v},t)=f_{0j}(\mathbf{r},\mathbf{v})+\tilde{f}_j(\mathbf{r},\mathbf{v},t)$ with the assumption that $\tilde{f}_j/f_{0j}\ll 1$. Retaining terms up to first order, we get

$$\left.\frac{D}{Dt}\right|_{u.t.p.} f_{0j}(\mathbf{r},\mathbf{v})=0, \quad \text{where}$$
$$\left.\frac{D}{Dt}\right|_{u.t.p.} \equiv \frac{\partial}{\partial t}+\mathbf{r}\cdot\nabla+\frac{q_j}{m_j}(\mathbf{v}\times\mathbf{B})\cdot\nabla_{\mathbf{v}}, \tag{1}$$

and

$$\left.\frac{D}{Dt}\right|_{u.t.p.} \tilde{f}_j(\mathbf{r},\mathbf{v},t)=-\frac{q_j}{m_j}E\cdot\nabla_{\mathbf{v}}f_{0j}. \tag{2}$$

Here $u.t.p$ implies unperturbed trajectories of particles, $\mathbf{B}=\nabla\times\mathbf{A}=B\hat{e}_\parallel$ is the equilibrium toroidal magnetic field, E is the perturbed electrostatic field, and q_j and m_j are the electric charge and mass of the species, respectively. Expressing $\tilde{\mathbf{E}}$ in terms of $\tilde{\varphi}$ and defining the following change of variables: $(\mathbf{r},\mathbf{v})\rightarrow(\mathbf{r},\xi=v^2/2,\mu=v_\perp^2/2B)$ and using particle canonical angular momentum for species j, i.e., $\psi_{0j}=\hat{e}_\phi\cdot[\mathbf{r}\times(\mathbf{A}+m_j\mathbf{v}/q_j)]=\psi+m_jrv_\phi/q_j$, one can write $f_{0j}(\mathbf{r},\mathbf{v})=f_{0j}(\mathbf{r},\xi,\mu,\psi_{0j})$. Here cylindrical coordinates $\mathbf{r}\equiv(r,\phi,z)$ have been introduced and $\psi=rA_\phi$ is the poloidal flux function per unit radian. Such a transformation would enable one to express f_{0j} in terms of single-particle constants of motion. Thus the $\nabla_{\mathbf{v}}f_{0j}$ term on the right-hand side $(r.h.s)$ of Eq. (2) becomes

$$\nabla_{\mathbf{v}} f_{0j}(\mathbf{r},\xi,\mu,\psi_{0j}) = \mathbf{v}\left(1+\frac{m_j r v_\phi}{q_j}\frac{\partial}{\partial\psi_{0j}}\right)\frac{\partial f_{0j\psi}}{\partial\xi}+\frac{\mathbf{v}_\perp}{B}\frac{\partial f_{0j\psi}}{\partial\mu} + \frac{m_j r\hat{e}_\phi}{q_j}\left.\frac{\partial f_{0j}}{\partial\psi_{0j}}\right|_{\psi_0=\psi}, \tag{3}$$

where $f_{0j\psi}\equiv f_{0j}(\psi_{0j}=\psi)$ and $\hat{e}_\phi$ is the toroidal unit vector. To obtain Eq. (3), f_{0j} is Taylor expanded to first order in $\{m_j r v_\phi/q_j\}$ around $\psi_{0j}=\psi$. Then, the following gyrokinetic ordering is used: $\omega/w_{cj}\ll 1, k_\perp \varrho_{Lj}\simeq O(1), k_\parallel \varrho_{Lj}\simeq \varrho_{Lj}/L_{\mathrm{eq}}$, where $k_\perp^{-1}, k_\parallel^{-1}, \varrho_{Lj}$ are perpendicular and parallel perturbation scales and Larmor radius of the species j, respectively, and L_{eq} is a typical equilibrium scale length. Rewriting $\tilde{f}_j$ in Eqs. (2), using the change of variables defined by

$$\tilde{f}_j = h_j^{(0)} + \tilde{\varphi}\frac{q_j}{m_j}\left[\left(1-\frac{v_\phi}{\Omega_{pj}}\nabla_n\right)\frac{\partial f_{0j\psi}}{\partial\xi}+\frac{1}{B}\frac{\partial f_{0j\psi}}{\partial\mu}\right], \tag{4}$$

and then invoking gyro-ordering followed by some standard vector algebra, we arrive at

$$\left.\frac{D}{Dt}\right|_{u.t.p} h_j^{(0)}(\mathbf{r},\mathbf{v},t) = -\frac{q_j}{m_j}\left[\frac{\partial f_{0j\psi}}{\partial\xi}\frac{\partial}{\partial t}+\frac{v_\parallel}{B}\frac{\partial f_{0j\psi}}{\partial\mu}\hat{e}_\parallel\cdot\nabla + \frac{1}{\Omega_{pj}}\nabla_n f_{0j}\left|_{\psi}\hat{e}_\phi\cdot\nabla\right.\right]\tilde{\varphi}+O(\epsilon). \tag{5}$$

In Eqs. (4) and (5), we have introduced the following definitions: $\Omega_{pj}=w_{cj}B_p/B$, $w_{cj}=q_jB/m_j$, $B_p=|\nabla\psi|/r$, and $h_j^{(0)}$ is the zeroth-order term of the perturbative series in the "inverse gyro-frequency expansion" of the nonadiabatic part $h_j=h_j^{(0)}+1/w_{cj}h_j^{(1)}+1/w_{cj}^2h_j^{(2)}\ldots$. Note that since $D/Dt\simeq O(w_{cj})$, only $h_j^{(0)}$ is retained, which is independent of w_{cj} and hence the gyro-angle (defined below). In the rest of this presentation, $h_j^{(0)}$ is referred to simply as h_j. Equation (5) is our starting equation. Now let us proceed with the gyro-averaging procedure. In a large aspect ratio tokamak geometry, the velocity $\mathbf{v}$ of a particle gyrating around a field line is $\mathbf{v}=v_\perp(\hat{e}_\varrho\cos\alpha+\hat{e}_\theta\sin\alpha)+v_\parallel\hat{e}_\parallel$, where unit vectors $(\hat{e}_\varrho,\hat{e}_\theta,\hat{e}_\phi)$ define the toroidal coordinates and α is the gyro-angle. We define gyro-averaging a quantity "Q" as

$$\langle Q\rangle = \frac{1}{2\pi}\int_0^{2\pi} d\alpha Q(\alpha;\ldots).$$

In Eq. (5), the terms in square brackets [...] on the right-hand side are all *equilibrium quantities* and are independent of α. Thus only the electrostatic potential is to be averaged. Similarly, on the left-hand side, h_j is independent of α, hence only $D/Dt|_{u.t.p}$ is to be gyro-averaged. Therefore,

$$\left.\frac{D}{Dt}\right|_{u.t.p} \overset{\text{gyro-averaging}}{\Rightarrow} \left.\frac{D}{Dt}\right|_{u.t.g} \equiv \frac{\partial}{\partial t}+(v_\parallel\hat{e}_\parallel+\mathbf{v_{dj}})\cdot\frac{\partial}{\partial\mathbf{R}},$$

where $\mathbf{v}_{dj}=(v_\perp^2/2+v_\parallel^2)\hat{e}_z/(rw_{cj})$, $u.t.g$ implies *unperturbed trajectory of guiding centers* $\mathbf{R}$ defined by $\mathbf{R}=\mathbf{r}+\mathbf{v}\times\hat{e}_\parallel/w_{cj}$. Therefore,

$$\langle\tilde{\varphi}\rangle = \left.\frac{1}{2\pi}\int_0^{2\pi} d\alpha[\tilde{\varphi}\ (\mathbf{r}[\alpha],t))]\right|_{\mathbf{r}=\mathbf{R}-\mathbf{v}\times\hat{e}_\parallel/w_{cj}}.$$

Since $\tilde{\varphi}(\mathbf{r}[\alpha],t)$ is an unknown function, the gyro-averaging is performed by first Fourier decomposing these functions, then representing the particle coordinate $\mathbf{r}$ by gyro-center $\mathbf{R}$ and remembering that

$$J_p(x) = \frac{1}{2\pi}\int_0^{2\pi} d\alpha\exp[\imath(x\sin\alpha - p\alpha)].$$

One can obtain a gyro-averaged equation for the nonadiabatic distribution function. With the above-mentioned procedure, one obtains the following *gyrokinetic equation*:

$$\left.\frac{D}{Dt}\right|_{u.t.g} h_j(\mathbf{R},\mathbf{v},t) = -\left(\frac{q_j}{m_j}\right)\left[\frac{\partial f_{0j\psi}}{\partial\xi}\frac{\partial}{\partial t}+\frac{v_\parallel}{B}\frac{\partial f_{0j\psi}}{\partial\mu}\hat{e}_\parallel\cdot\nabla + \frac{1}{\Omega_{pj}}\nabla_n f_{0j}\left|_{\psi}\hat{e}_\phi\cdot\nabla\right.\right] \times(\tilde{\varphi}(\mathbf{k};)J_0(k_\perp\varrho_{Lj}))+O(\epsilon). \tag{6}$$

The solution to Eq. (6) is obtained by the *Green function technique* (unit source solution, *say* $\mathcal{P}$).[25] An explicit form of $\mathcal{P}$ is obtained analytically by the method of characteristics of unperturbed trajectories of guiding centers $(u.t.g)$ and followed by a perturbative technique for the guiding center velocity.[5] Moreover, the unit source solution, $\mathcal{P}$, to Eq. (6) is independent of the type of perturbation (electrostatic or electromagnetic) and solely depends on the considered *equilibrium*. We assume for equilibrium, f_{0j}, a local Maxwellian of the form

$$f_{0j}(\xi,\mu,\psi) = f_{Mj}(\xi,\psi) = \frac{N(\psi)}{\left(\frac{2\pi T_j(\psi)}{m_j}\right)^{3/2}}\exp\left(-\frac{\xi}{T_j(\psi)/m_j}\right)$$

so that $\partial f_{0j}/\partial\mu\equiv 0$ by choice and density profile $N(\psi)$ is independent of the species type j. Thus, for a "sinusoidal" time dependence, the solution to Eq. (6) in guiding center coordinates $\mathbf{R}$ is

$$h_j(\mathbf{R},\mathbf{v},\omega) = -\left(\frac{q_jF_{Mj}}{T_j}\right)\int d\mathbf{k}\exp(\imath\mathbf{k}\cdot\mathbf{R}(\omega-\omega_j^*)) \times(\imath\mathcal{P}_j)\tilde{\varphi}(\mathbf{k};)J_0(k_\perp\varrho_{Lj})+O(\epsilon).$$

Here, $\mathbf{k}=\kappa\hat{e}_\rho+k_\theta\hat{e}_\theta+k_\phi\hat{e}_\phi$ and $\kappa=(2\pi/\Delta\rho)k_\rho$, with $\Delta\rho=\rho_u-\rho_l$, which defines the radial domain, $k_\phi=n/r$ and $k_\theta=m/\rho$; ω is the *eigenvalue* and $\omega_j^*=\omega_{nj}[1+\eta_j/2(v_\parallel^2/v_{thj}^2-3)+\eta_jv_\perp^2/2v_{thj}^2]$ with $\omega_{nj}=(T_j\nabla_n\ln Nk_\theta)/(q_jB)$ is the *diamagnetic drift frequency*; $\eta_j=(d\ln T_j)/(d\ln N)$. Note also that since the large aspect ratio equilibria considered are axisymmetric, the toroidal mode number "n" can be fixed and the problem is effectively two-dimensional in (ρ,θ) (configuration space) or (κ,k_θ) (Fourier space).

As our interest is in nonadiabatic passing electrons, let us now proceed to the construction of the propagator for passing gyrokinetic species (For trapped ions, see Ref. 5). Since a gyro-averaged Vlasov equation can be solved using a

method of integrating along its $u.t.g$, for our special class of "sinusoidal" time dependence, the solution $\mathcal{P}$ for a given $(\mathbf{k},\omega)$ is simply

$$\mathcal{P}(\mathbf{R},\mathbf{k},\epsilon,\mu,\sigma,\omega)=\int_{-\infty}^{t}dt'\,\exp(\iota[\mathbf{k}\cdot(\mathbf{R}'-\mathbf{R})-\omega t'])$$
$$=\int_{-\infty}^{t}dt'\,\exp\left(\iota\int^{t'}dt''\mathbf{k}\cdot\mathbf{v}_g(t'')-\iota\omega t'\right), \tag{7}$$

where the guiding center velocity $d\mathbf{R}/dt=\mathbf{v}_g=\mathbf{v}_\parallel+\mathbf{v}_d$, and $\mathbf{R}(t)$ is to be obtained by solving for guiding center trajectories as an "initial value problem" in equilibrium considered above. This is done by first assuming that the cross-field drift terms $[\mathbf{v}_d]$ are small and drop them at the zeroth order and to include them iteratively at the next order. This procedure gives us $\mathcal{P}$,

$$\iota\mathcal{P}=\sum_{p,p'}\frac{J_p(x_{tj}^\sigma)J_{p'}(x_{tj}^\sigma)}{\omega-\sigma k_\parallel v_\parallel-p\omega_t}\exp(\iota(p-p')(\theta-\bar{\theta}_\sigma)), \tag{8}$$

where $x_{tj}^\sigma=k_\perp\xi_\sigma$, $\xi_\sigma=v_d/\omega_t, v_d=(v_\perp^2/2+v_\parallel^2)/(\omega_c R),\omega_t=\sigma v_\parallel/(q(s)R),\sigma=\pm1$ (sign of $\mathbf{v}_\parallel$), $k_\perp=\sqrt{\kappa^2+k_\theta^2}$, $k_\parallel=[nq(s)-m]/(q(s)R)$, and $\bar{\theta}_\sigma$ is defined as $\tan\bar{\theta}_\sigma=-\kappa/k_\theta$ and $s=\rho/a$, $a-$ is the minor radius. A few points to be noted here are as follows: (1) Note that the grad-B and curvature drift effects appear through the argument of Bessel functions $(x_{tj}^\sigma=k_\perp v_d/\omega_t)$ of Eq. (8). Thus for example, "radial and poloidal coupling" vanishes if $x_{tj}^\sigma=0$ in Eq. (8) and one would arrive at "cylindrical" results. Hence in our model, Bessel functions in Eq. (8) bring about coupling between neighboring flux surfaces and also couple neighboring poloidal harmonics. (2) The argument of Bessel functions J_p's in Eq. (8), i.e., $x_{tj}^\sigma=k_\perp\xi_\sigma$, also depends on transit frequency ω_t, x_{tj}^σ can become $x_{tj}\simeq\mathcal{O}(1)$. Hence transit harmonic orders are to be chosen accordingly. In this form, $\mathcal{P}$ contains effects such as transit harmonic and its coupling, parallel velocity resonances, and poloidal mode coupling.

To obtain the particle density fluctuation $\tilde{n}_j(\mathbf{r};\omega)$, one needs to go from guiding center (GC) coordinate $\mathbf{R}$ to *particle coordinate* $\mathbf{r}$ using $\mathbf{R}=\mathbf{r}+\mathbf{v}\times\hat{e}_\parallel/w_{cj}$, by replacing h_j using Eq. (4) followed by the integration over $\mathbf{v}$ keeping in mind the *gyro-angle* integration over α. This last integration on α yields an additional Bessel function "J_0 for $\tilde{\varphi}$. Thus, in real space $\mathbf{r}$, for species j, we finally have

$$\tilde{n}_j(\mathbf{r};\omega)=-\left(\frac{q_jN}{T_j}\right)\left[\tilde{\varphi}+\int d\mathbf{k}\exp(\iota\mathbf{k}\cdot\mathbf{r})\times\int d\mathbf{v}\frac{f_{Mj}}{N}(\omega-\omega_j^*)(\iota\mathcal{P}_j)\tilde{\varphi}(\mathbf{k};)J_0^2(x_{Lj})\right],$$

where $x_{Lj}=k_\perp\varrho_{Lj}$. It may be worthwhile to emphasize that equilibrium effects (incorporated in $\mathcal{P}$) and perturbation effects are clearly delineated in the formulation. Equations are finally closed by invoking the *quasineutrality condition*,

$$\sum_j\tilde{n}_j(\mathbf{r};\omega)\simeq0. \tag{9}$$

Equation (9) defines a generalized eigenvalue problem with eigenvalue ω and eigenvector $\tilde{\varphi}$. This eigenvalue problem is conveniently solved in Fourier space. By Fourier decomposing the potential in Eq. (9) and then taking Fourier transform, we obtain a convolution matrix in Fourier space. If we assume a hydrogen-like plasma with ions, electrons, and trapped ions, we have

$$\sum_{\mathbf{k}'}\sum_{j=i,e,\mathrm{tr}-i}\hat{\mathcal{M}}_{\mathbf{k},\mathbf{k}'}^j\tilde{\varphi}_{\mathbf{k}'}=0,$$

where $\mathbf{k}=(\kappa,m)$ and $\mathbf{k}'=(\kappa',m')$. Note that we have three species: Passing ions (i), passing electrons (e), and trapped ions $(tr\text{-}i)$. In the following, we discuss in detail the formulation for passing species. For trapped ions, the reader is referred to Ref. 4. With the following definitions, $\Delta\rho=\rho_u-\rho_l$ (upper and lower radial limits), $\Delta_\kappa=\kappa-\kappa'$, and $\Delta_m=m-m'$ matrix elements are

$$\hat{\mathcal{M}}_{\mathbf{k},\mathbf{k}'}^i=\frac{1}{\Delta\rho}\int_{\rho_l}^{\rho_u}d\rho\exp(-\iota\Delta_\kappa\rho)\times\left[\alpha_p\delta_{mm'}+\exp(\iota\Delta_m\bar{\theta})\sum_p\hat{I}_{p,i}^0\right],$$
$$\hat{\mathcal{M}}_{\mathbf{k},\mathbf{k}'}^e=\frac{1}{\Delta\rho}\int_{\rho_l}^{\rho_u}d\rho\exp(-\iota\Delta_\kappa\rho)\times\left[\frac{\alpha_p}{\tau(\rho)}\delta_{mm'}+\frac{\exp(\iota\Delta_m\bar{\theta})}{\tau(\rho)}\sum_p\hat{I}_{p,e}^0\right], \tag{10}$$

where

$$\hat{I}_{p,j}^l=\frac{1}{\sqrt{2\pi}v_{\mathrm{th},j}^3(\rho)}\int_{-v\max_j(\rho)}^{v\max_j(\rho)}v_\parallel^l dv_\parallel\exp\left(-\frac{v_\parallel^2}{v_{\mathrm{th},j}^2(\rho)}\right)\times\left\{\frac{N_1^jI_{0,j}^\sigma-N_2^jI_{1,j}^\sigma}{D_1^{\sigma,j}}\right\}_{p'=p-(m-m')},$$

$$I_{n,j}^\sigma=\int_0^{v_{\perp\max,j(\rho)}}v_\perp^{2n+1}dv_\perp\times\exp\left(-\frac{v_\perp^2}{2v_{\mathrm{th},j}^2(\rho)}\right)J_0^2(x_{Lj})J_p(x_{tj}'^\sigma)J_{p'}(x_{tj}'^\sigma).$$

We have introduced the following definitions: $v_{\perp\max,j(\rho)}=\min(v_\parallel/\sqrt{\epsilon},v_{\min,j})$ which is "trapped particle exclusion" from ω independent perpendicular velocity integral $I_{n,j}^\sigma$; $\alpha_p=1-\sqrt{\epsilon/(1+\epsilon)}$ is the fraction of passing particles; $\hat{I}_{p,j}^l$ is ω-dependent parallel integrals; $x_{tj}^\sigma=k_\perp\xi_\sigma$, $N_1^j=\omega-w_{n,j}[1+(\eta_j/2)(v_\parallel^2/v_{\mathrm{th},j}^2)-3)]$; $N_2^j=w_{n,j}\eta_j/(2v_{\mathrm{th},j}^2)$ and $D_1^{\sigma,j}=<w_{t,j}(\rho)>(nq_s-m'(1-p)(\sigma v_\parallel/v_{\mathrm{th},j})-\omega$, where $<w_{t,j}(\rho)>=v_{\mathrm{th},j}(\rho)/(rq_s)$ is the average *transit frequency* of the species j. As integrals $I_{n,j}^\sigma$ are independent of ω and dependent only on $v_\perp$, σ, and other equilibrium quantities, one may choose to calculate and store them as interpolation tables (memory intensive) or, alternatively, one may choose to cal-

TABLE I. Equilibrium profiles and parameters.

Parameters	Equilibrium Profiles
• B-field: $B_0=1.0$ T	• N-profile and T-profile
• Temperature: $T_0=T(s_0)=7.5$ keV	$N(s)/N_0=\exp\left(-\frac{a}{L_{n0}}\frac{\delta s_n}{\tanh\left(\frac{s-s_0}{\delta s_n}\right)}\right)$
• Major radius: $R=2.0$ m	$T_{i,e}(s)/T_0=\exp\left(-\frac{a}{L_{T0}}\frac{\delta s_T}{\tanh\left(\frac{s-s_0}{\delta s_T}\right)}\right)$
• Minor radius: $a=0.5$ m	$\delta s_n=0.35$, $\delta s_T=0.2$ at $s=s_0$
• Radius: $s=\rho/a$ $0.01<s<1.0$, $s_0=0.6$	• $q(s)=1.25+0.67\ s^2+2.38\ s^3-0.06\ s^4$ such that $q(s=s_0)=2.0$;
• $L_{n0}=0.4$ m, $L_{T0}=0.2$ m $\rightarrow \eta_{i,e}(s_0)=2.0$	Shear $\hat{s}$ is positive and at $s=s_0$, $\hat{s}=1$.
• $\tau(s)=T_e(s)/T_i(s)=1$.	

culate them when needed (CPU-time-intensive). Various numerical convergence tests have been performed with a number of radial and poloidal Fourier modes, equilibrium profile discretization, and velocity integrals. In the next section, we will specify some diagnostics and normalizations used in the code.

A. Diagnostics: Eigenmode-averaged quantities

Simple diagnostics for various physical quantities are computed as averages over the eigenmode. For example, mode-averaged k_θ^2 is computed as

$$\langle k_\theta^2 \rangle = \frac{\int d\rho \sum_m \left| \frac{m}{\rho} \varphi_{(k,m)} \right|^2}{\int d\rho \Sigma_m |\varphi_{(k,m)}|^2}, \tag{11}$$

where quantities with suffix "(k,m)" imply Fourier weights of corresponding perturbations.

B. Normalization for full radius calculation

Distances are normalized to minor radius "a," i.e., $s=\rho/a$. Radial position where η_j peaks is represented as $s=s_0$. Frequencies and growth rates are normalized to $\omega_{d0}=v_{\rm thi}(s=s_0)\varrho_{\rm Li}/a^2$, $k_\perp$ is normalized to its local (ion/electron) inverse Larmor radius $\varrho_{Lj}^{-1}(s)$, $k_\parallel$ to L_n^{-1} (inverse density gradient length scale), magnetic field B to $B(s=0)$, density to $N(s=s_0)$, temperature T to $T(s=s_0)$, and velocities $(v_\perp, v_\parallel)$ to $v_{\rm thi}(s)$ (i.e., to their radially local thermal values).

All input quantities to the code EM-GLOGYSTO are in SI units, except the temperature of given species, which is in eV. Hence, for example, $v_{\rm thi}$ is computed using $v_{\rm thi}^2(\text{in m/s})=T_i(\text{in Joule})/m_i(\text{in Kg})=|e|T_i(\text{in eV})/m_i(\text{in Kg})$, where $|e|$ is the absolute value of electronic charge. Thus, for example, for parameters throughout this work, we have $\omega_{d0}\simeq 3\times 10^4\ \text{s}^{-1}$.

III. RESULTS AND DISCUSSION

We choose DII-D-like profiles and parameters (Table I) to demonstrate the effect of nonadiabatic passing electrons on global ITGs.

For these parameters, equilibrium profiles are shown in Fig. 1. For the above-mentioned parameters, $\rho^* \equiv \rho_{\rm Li}(s=s_0)/a \simeq 0.0175$.

A. *n*-scan: Effect of variation of η_e, multiscale features, and mixing length transport

Growth rates γ and real frequencies ω_r of global ITG mode as functions of plasma toroidal mode number n are shown in Fig. 2. Usual adiabatic electron response $(\tilde{n}_e=n_0 e\phi/T_e)$ is shown with solid lines, whereas results with a nonadiabatic model for various values of η_e are shown by dashed lines with open and filled circles. The growth peaks around $n=8,9$. This result shows that electron nonadiabaticity indeed affects the growth rates, in general. For finite time taken by passing electrons to respond to $\mathbf{E}$ perturbations, especially in regions where the magnetic surface is mode-rational, $k_{\parallel m,n}\simeq 0$, the nonadiabatic contribution is significant.

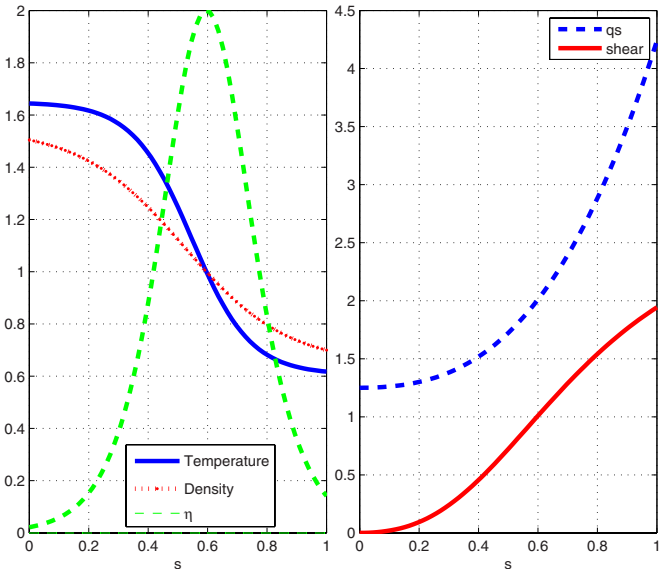

FIG. 1. (Color online) Equilibrium profiles for global ITG stability studies (parameters for the table): Normalized density, temperature, and $\eta_{i,e}$ (left) and safety factor q and magnetic shear $\hat{s}$ profiles as functions of normalized radius $s=r/a$. Note that η peaks at $s=\rho/a=s_0=0.6$.

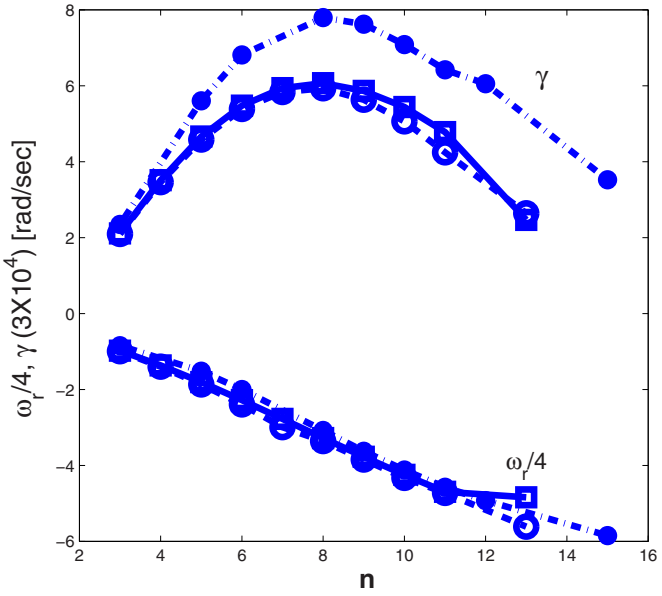

FIG. 2. (Color online) (a) Growth rates and (b) frequencies for profiles in Fig. 1: Growth rate γ and real frequency ω_r for $\eta_i(s_0)=2$ with adiabatic electron model (□), with nonadiabatic electron model at $\eta_e(s_0)=2.0$ (○), and $\eta_e(s_0)=8$ (●).

To elucidate this idea, for $\eta_i=2.0$, we have computed the global eigenmode structures of global ITG at $n=9$, where the growth rate peaks. Again, for electrons we have two cases: (i) Adiabatic electron response and (ii) nonadiabatic electron response with various values for η_e. For example, in Fig. 3, eigenmode structures for the adiabatic electron case are compared with the nonadiabatic electron response with $\eta_e=2$.

The "ballooning" nature of the modes on the "bad curvature" region is also clearly demonstrated. For example, unlike a "cylindrical" or "slab" ITG, here for each value of n there are about 10 poloidal mode numbers m coupled. This is again seen in Fig. 4, where at a radial location, say $s=r/a=0.6$, one can see a predominant Fourier contribution from several m numbers. The global nature of the mode is adequately demonstrated by projecting the eigenmode onto the poloidal plane. The mode width indeed occupies about 30% of the minor radius a extending over several mode-rational surfaces $r=r_{\mathrm{MRS}}$.

Note that at locations where $k_{\|m,n}=0$, the mode structure is very sharp for ITGs with nonadiabatic electrons, whereas no such effect is detectable for the ITGs with the usual adiabatic electrons. Consequently, the radial wavenumbers k_r needed to be resolved increases, as seen in Fig. 5.

To understand the structures, let us look at the mode-rational surfaces and phase velocity $v_{m,n}^{ph}$ across the entire minor radius for equilibrium q profiles shown in the above table (Fig. 1). In Fig. 6, for $n=9$, $\omega_r/k_{\|m,n}$, the per-mode phase velocity is plotted as a function of normalized radius along with v_{the} and v_{thi}. If one assumes adiabatic electron response, as is usually done, then in both rapidly increasing regions of $v_{m,n}^{ph}$ (i.e., as $r\to r_{\mathrm{MRS}}$) as well as in regular regions ($r\neq r_{\mathrm{MRS}}$), electrons are "forced" to respond "instantaneously." However, as can be seen from Fig. 6, in regions close to $r=r_{\mathrm{MRS}}$, electrons cannot respond instantaneously, but take finite time to respond. Thus if the correct nonadiabatic response is incorporated, then for all radial locations (i.e., for all per-mode phase velocities), there would be appropriate electron response. For example, for regions $r\neq r_{\mathrm{MRS}}$, where $v_{m,n}^{ph}$ is small compared to $v_{\mathrm{the}}(r)$, automatically the response will be adiabatic. In the same way, as $r\to r_{\mathrm{MRS}}$, the local phase velocity increases and hence strong deviations from nonadiabaticity occur, which will be auto-

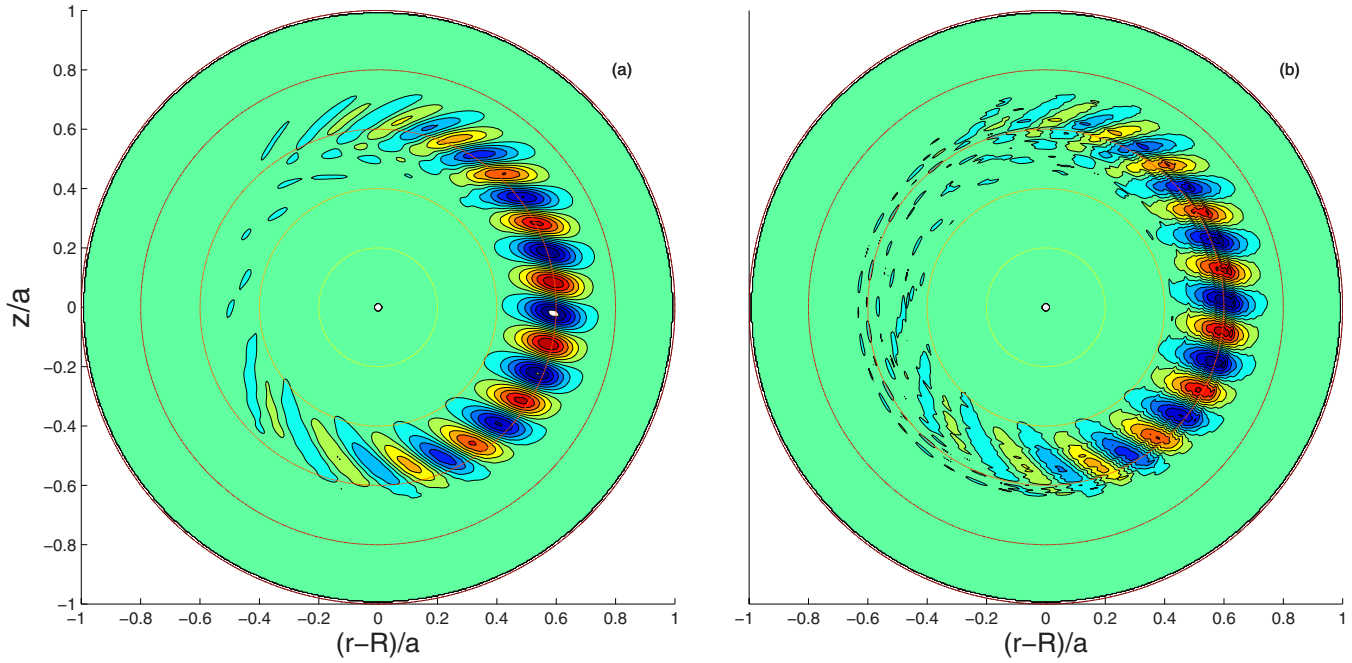

FIG. 3. (Color online) Two-dimensional eigenmode structure of global ITG at $n=9$, $\eta_i(s_0)=2$ for adiabatic electron response (left column) and nonadiabatic electron response (right column) at $\eta_e(s_0)=2$. The global nature of the mode is clearly visible, covering about 30% of the minor radius.

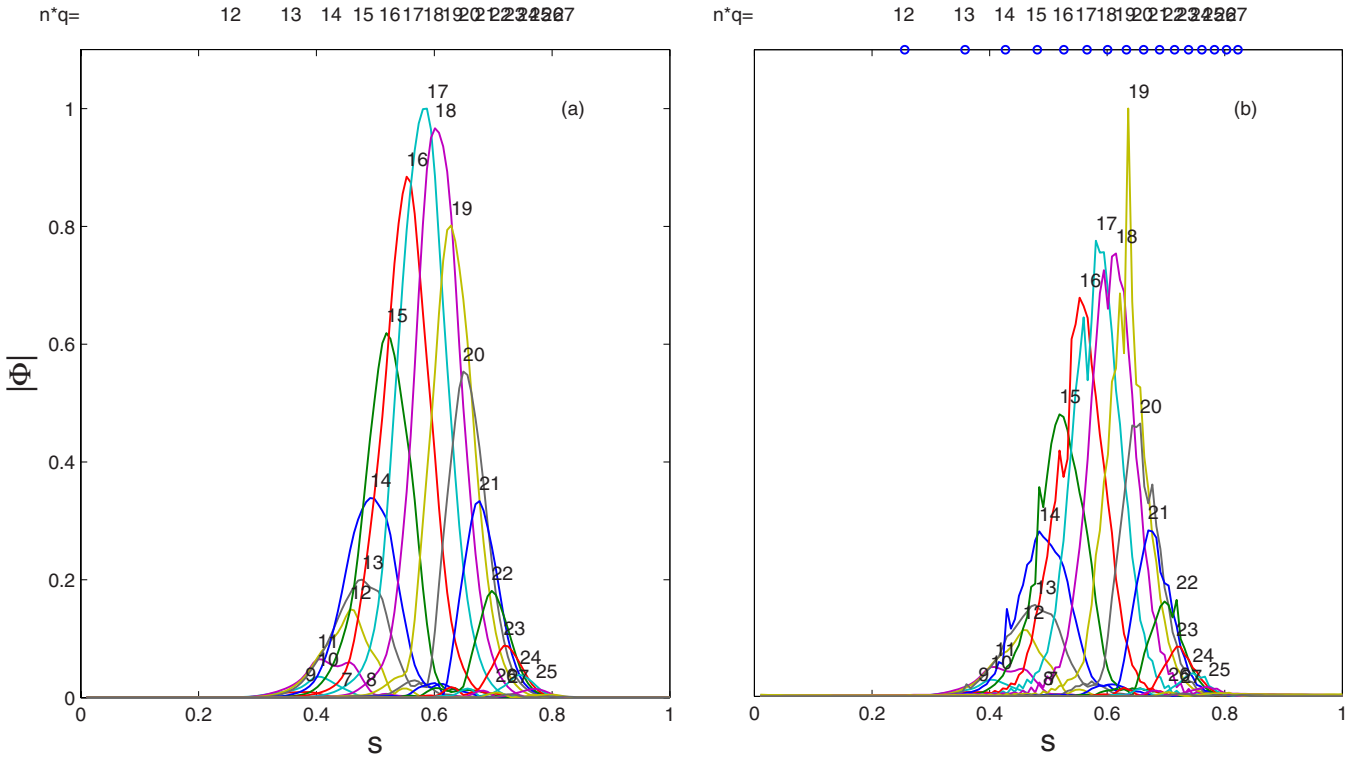

FIG. 4. (Color online) Poloidal Fourier components for the electrostatic mode shown in Fig. 3. Note that at each radial location, there are several poloidal harmonics coupled. The location where $k_{\|m,n}=0$ (i.e., $nq=m$) is indicated on the top axis. Nonadiabatic electrons introduce sharp structure near these points.

matically accounted for. Such nonadiabatic effects are indeed important for global ITGs as they alter both the growth rate and the mode structures remarkably.

An alternate way of understanding this situation is as follows: Nonadiabatic electron response allows residual nonneutralized E field, and introduces phase delay between density and potential fluctuations and the concomittant growth. Multiscale features seen in mode structure may remind one of nonlinear effects such as zonal flows, which "break up" the modes resulting in slower rates of growth for ITGs. However, here the exact opposite happens. Linear mode structure is "broken up" due to linear nonadiabatic response of electrons introducing phase delays and thus pronounced growth. In Fig. 7, we show a close-up of global eigenmodes with adiabatic electron response and with nonadiabatic electron response.

These multiscale structures in turn increase the effective or mode-averaged wavenumber as compared to the adiabatic electron model. For example, eigenmode averaged $k_r\rho_{\mathrm{Li}}$, $k_\theta\rho_{\mathrm{Li}}$, and $k_\perp\rho_{\mathrm{Li}}$ for the adiabatic electron model, the nonadiabatic electron model at $\eta_e=2$ and $\eta_e=8$ are shown in Fig. 8 for various values of n. Note that due to the sharp radial structure introduced by nonadiabatic electrons, the effective $k_\perp\rho_{\mathrm{Li}}$ has been enhanced in both cases of η_e. It would then be interesting to construct the so-called "mixing length" transport for transport coefficient, $D_{ML}=\gamma/\langle k_\perp^2\rangle$ from the lin-

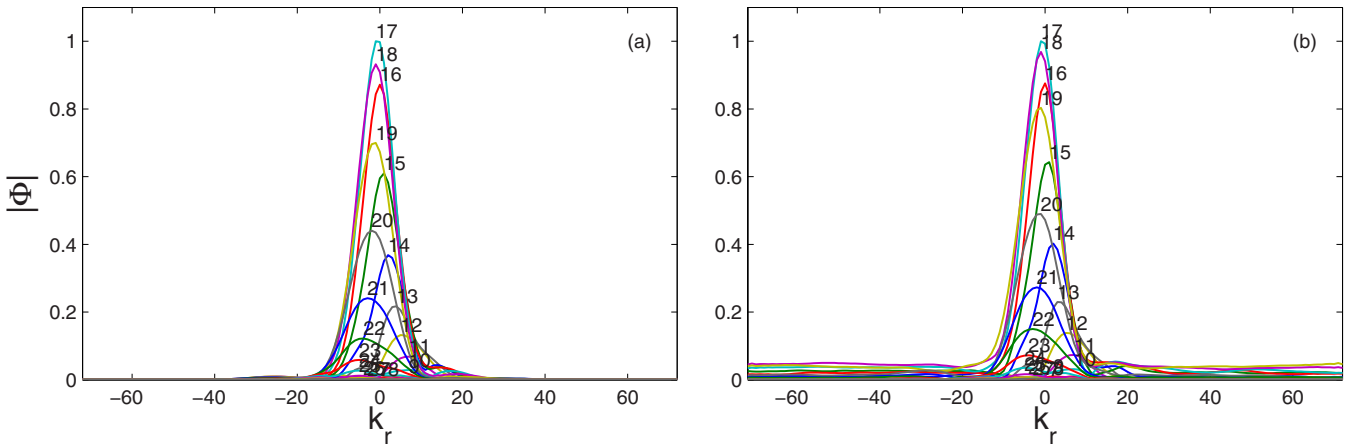

FIG. 5. (Color online) Radial Fourier harmonics for each poloidal mode for the electrostatic mode shown in Fig. 3. Here we have used 144 modes. For numerical convergence, we have tested with a larger number of radial harmonics and we observed that the results are converged. Convergence is not shown.

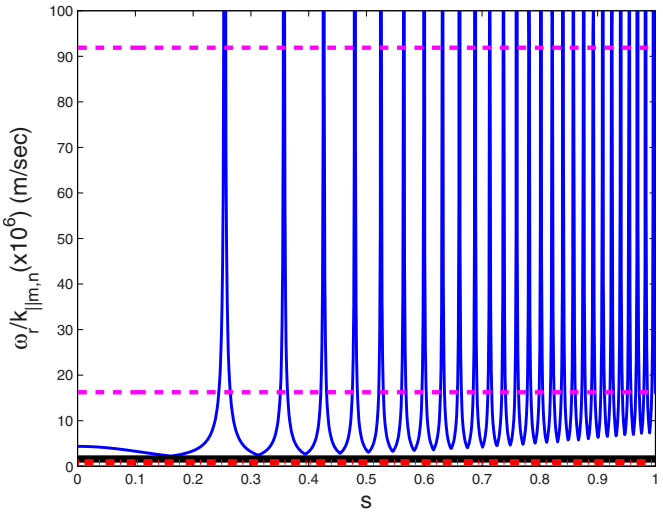

FIG. 6. (Color online) Typical per-mode phase velocity $\omega_r/k_{\|m,n}$ vs normalized minor radius $s=r/a$ for the equilibrium profile of q shown in Fig. 1 with $\eta_e(s_0)=8$, $\eta_i(s_0)=2$, $n=9$. Location of peaks ($r=r_{mrs}$) indicate mode rational surfaces. Horizontal dashed lines are electron thermal velocities v_{the} at radial locations at the beginning ($s=0.4$) and end ($s=0.7$) of mode structure. There are two overlapping lines for ions. Horizontal dashed-dotted lines are ion thermal speeds and continuous line is eigenmode averaged, i.e., global phase velocity $\langle \omega_r/k_{\|m,n}\rangle$.

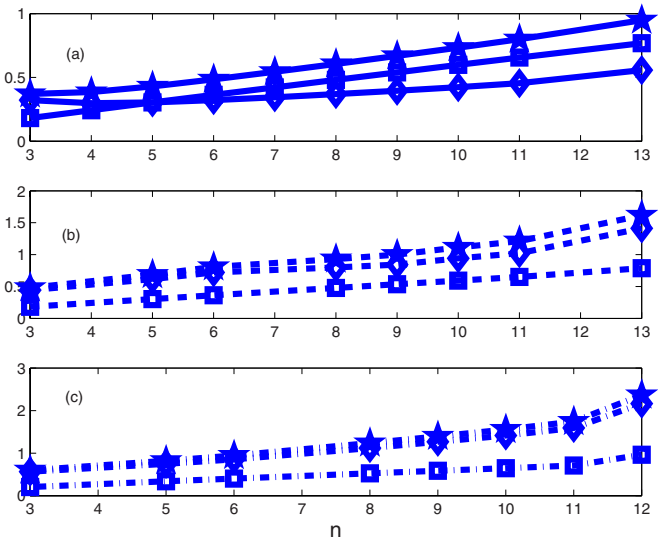

FIG. 8. (Color online) Eigenmode averaged normalized mode numbers $\langle k_\theta \rho_{\text{Li}}\rangle$ (□), $\langle k_r \rho_{\text{Li}}\rangle$ (◇), and $\langle k_\perp \rho_{\text{Li}}\rangle$ (★) as a function of toroidal mode number n at $\eta_i(s_0)=2$; (a) adiabatic electron response and (b) nonadiabatic electron response at $\eta_e(s_0)=2$. (c) Same as in (b) at $\eta_e(s_0)=8$.

ear growth rate γ and mode-averaged $k_\perp$, i.e., $\langle k_\perp\rangle$. In Fig. 9, we present the mixing-length estimates in the usual gyro-Bohm units as a function of the toroidal mode number n. It is found that compared to the adiabatic electron model, the transport predicted from global ITGs for nonadiabatic electrons results in a reduction in transport. It is important to note that the presence of nonadiabatic trapped electrons[4] may alter the levels of transport observed here due to nonadiabatic passing electrons. Such a study remains to be addressed.

It may be of interest to note that both nonlinearly generated zonal flows and linear but nonadiabatic passing electrons "break up" the mode structures. While the zonal flow breakup is not related to any particular surface ($k_\|=0$ everywhere for the $m=0, n=0$ zonal flow potential perturbation), the presently studied effect occurs due to $m\neq 0$, $n\neq 0$ but $k_\|=0$ mode-rational surfaces.

B. η_i scan: Nonadiabatic electrons cause a downshift of critical η_i

Next, we study the effect of nonadiabatic passing electrons on the critical ion temperature gradient parameter η_i. For adiabatic electrons, global ITGs are known to destabilize at about $\eta_{i,\text{crit}}=1.1$. Here, we follow the highest growth rate mode, namely $n=9$, and we investigate the smallest value of η_i at which this mode becomes unstable. We have studied again three cases: (i) Global ITGs with adiabatic electrons, (ii) with nonadiabatic electrons at $\eta_e=2$, and finally (iii) with nonadiabatic electrons with $\eta_e=8$. We find that the critical η_i is *reduced* compared to the adiabatic electron model. This result is perhaps not surprising. As we have seen in the preceding section, nonadiabatic electrons tend to further destabilize global ITGs as compared to global ITGs with adiabatic electrons. Hence one may expect that a relatively weaker ion temperature gradient would destabilize global ITGs now as compared to the adiabatic model. This expectation is indeed shown to be true in Fig. 10. Physics-wise, this result implies that, for example, for similar density profiles, in tokamaks

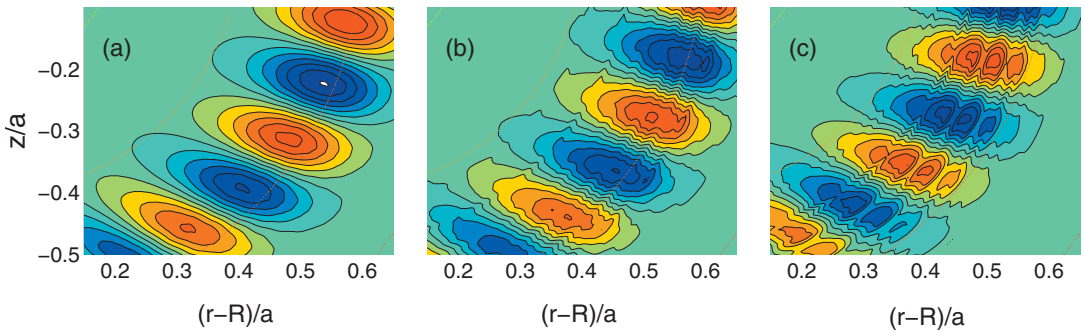

FIG. 7. (Color) Closeup of the two-dimensional eigenmode structure of global ITG at $n=9$, $\eta_i=2$ for (a) adiabatic electron response and (b) nonadiabatic electron response at $\eta_e(s_0)=2$. (c) Same as in (b) at $\eta_e=8(s_0)$.

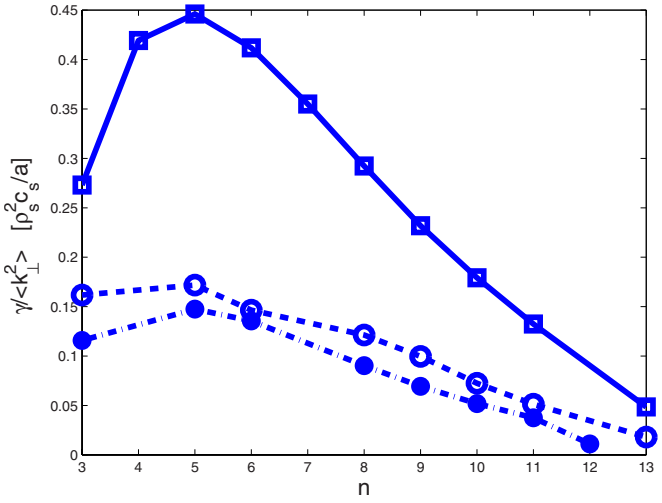

FIG. 9. (Color online) Mixing length estimate for transport coefficient $D_{ML}=\gamma/\langle k_\perp^2\rangle$ in gyro-Bohm units as a function of toroidal mode number n; $\eta_i(s_0)=2$ for (a) adiabatic electron response (solid line) and (b) nonadiabatic electron response at $\eta_e(s_0)=2$ (dashed line). (c) Same as in (b) at $\eta_e(s_0)=8$ (dot-dashed line).

with steeper electron temperature gradient than ions, global ITGs would become unstable for smaller values of η_i than predicted by adiabatic electron models. Thus downshifting critical η_i. This linear phenomenon is in contrast to upshifting of critical η_i when nonlinear zonal flows are allowed to evolve simultaneously with ITGs.[26,27]

IV. CONCLUSION

We have presented a 2D global gyrokinetic stability study as applicable to large aspect ratio tokamaks. We have focused on the effect of treating electrons on the same physics footing as ions, meaning fully nonadiabatic electrons. For this study, we have included passing ions, trapped ions, and passing electrons. The model includes arbitrary order FLR effects, kinetic effects such as Landau damping, transit/trapped particle resonances, poloidal and radial coupling, and magnetic resonances. With the above-mentioned model for electrons, we have reported the study of global toroidal ITGs for low toroidal mode numbers in the range $3<n<15$. There are several interesting new results:

1. For nearly the same values of η_i and η_e, the global mode structure is observed to change dramatically. With increasing η_e values, i.e., with more nonadiabaticity, growth rates also are seen to increase. Thus, we conclude that, in general, nonadiabatic passing electron dynamics destabilize global ITGs.
2. Important structural changes in the eigenmode structure appear near the mode-rational surfaces where per-mode $k_{\|m,n}$ vanishes. On these surfaces, the local phase velocity grows quickly. Because the mode is global and spans across several mode rational surfaces, generalizing electron dynamics, as done in the present study, introduces a multiscale nature in global ITG eigenmodes. These effects in turn alter the effective $k_\perp$. A combination of these effects appears to bring down the mixing length transport estimates as compared to global ITGs with adiabatic electron dynamics.
3. Finally, an important fall out is the downshift of critical η_i values as compared to the adiabatic electron model.

As discussed in the Introduction, trapped nonadiabatic electrons are only beginning to be modeled using time-dependent particle or Vlasov methods. However, passing nonadiabatic electrons are responsible for bulk electric currents and their fluctuations. Assuming that both sophisticated computing abilities as well as advanced physics modeling will allow one to handle nonadiabatic passing electron dynamics in the future, then we believe that our model presented here would serve as a minimal nontrivial benchmark for such time-dependent linear/nonlinear gyrokinetic particle or Vlasov codes.

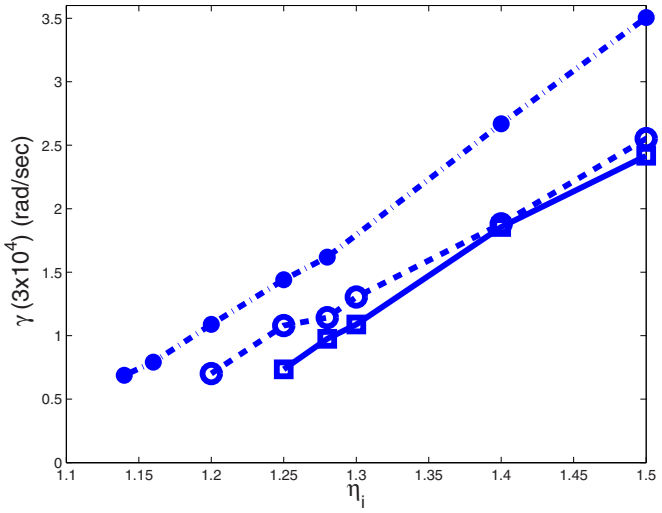

FIG. 10. (Color online) For the highest growth rate mode toroidal mode number $n=9$, η_i scan is performed for three cases of electron model: (a) Adiabatic electron response (solid line) and (b) nonadiabatic electron response at $\eta_e(s_0)=2$ (dashed line). (c) Same as in (b) at $\eta_e(s_0)=8$ (dot-dashed line). Results clearly show that $\eta_{i,\mathrm{crit}}$ is downshifted.

ACKNOWLEDGMENTS

J.C. and R.G. are thankful to R. Singh and P. K. Kaw for very useful discussions and a careful reading of the manuscript. They are also thankful to IPR Computer Centre for its support during the course of this work. All the work was performed on a 34-node Xeon cluster with fast-ethernet interconnect at IPR. The CRPP authors were partly supported by the Swiss National Science Foundation.

[1] L. I. Rudakov and R. Z. Sagdeev, Nucl. Fusion Suppl. **2**, 481 (1962).
[2] M. N. Rosenbluth and M. L. Sloan, Phys. Fluids **14**, 1725 (1971).
[3] A. B. Mikhailovskii, Nucl. Fusion **13**, 259 (1973).
[4] S. Brunner, M. Fivaz, T. M. Tran, and J. Vaclavik, Phys. Plasmas **5**, 3929 (1998).
[5] S. Brunner, Ph.D. thesis, EPFL, Switzerland (1997).
[6] M. Fivaz, T. M. Tran, L. Villard, K. Appert, S. Brunner, S. E. Parker, and J. Vaclavik, in *Theory of Fusion Plasmas, International Workshop, Varenna, August, 1996* (Editrice Compository, Societa Italiana di Fisica, Bologna, 1997).
[7] G. L. Falchetto, J. Vaclavik, and L. Villard, Phys. Plasmas **10**, 1424 (2003).
[8] P. Angelino, A. Bottino, G. Falchetto, R. Ganesh, J. Vaclavik, and L. Villard, Transp. Theory Stat. Phys. **34**, 333 (2005).

[9]R. Ganesh, J. Vaclavik, and L. Villard, in *Proceedings of the Joint Varenna-Lausanne International Workshop on Theory of Fusion Plasmas, Villa Monastero-Varenna, Italy, 2004*, edited by J. W. Connor, O. Sauter, and E. Sindoni (Societa Italiana Di Fisica, Italy 2004).
[10]R. Ganesh, P. Angelino, J. Vaclavik, and L. Villard, Phys. Plasmas **11**, 3106 (2004).
[11]R. Ganesh and J. Vaclavik, Phys. Rev. Lett. **94**, 145002 (2005).
[12]W. M. Tang, Nucl. Fusion **18**, 1089 (1978).
[13]W. M. Tang, J. Connor, and R. J. Hastie, Nucl. Fusion **21**, 1439 (1980).
[14]C. Z. Cheng, Phys. Fluids **25**, 1020 (1982); Phys. Rep. **211**, 1 (1992).
[15]M. Kotschenreuther, Phys. Fluids **29**, 2898 (1986).
[16]F. Zonca, L. Chen, J. Q. Dong, and R. A. Santoro, Phys. Plasmas **6**, 1917 (1999).
[17]P. Angelino, Ph.D. thesis, EPFL, Switzerland (2006).
[18]W. D. Dorland, Ph.D. thesis, Princeton University (1993).
[19]M. A. Beer and G. W. Hammett, Phys. Plasmas **3**, 4018 (1996).
[20]B. H. Fong and T. S. Hahm, Phys. Plasmas **6**, 188 (1999).
[21]W. W. Lee, J. L. V. Lewandowski, T. S. Hahm, and Z. Lin, Phys. Plasmas **8**, 4435 (2001).
[22]P. J. Catto, W. M. Tang, and D. E. Baldwin, Phys. Fluids **23**, 639 (1981).
[23]T. S. Hahm, W. W. Lee, and A. Brizard, Phys. Fluids **31**, 1940 (1988).
[24]A. J. Brizard, Phys. Rev. Lett. **84**, 5768 (2000).
[25]N. A. Krall and A. W. Trivelpiece, *Principles of Plasma Physics* (San Francisco, San Francisco, 1986), pp. 396–397.
[26]P. Terry, Rev. Mod. Phys. **72**, 109 (2000).
[27]P. H. Diamond, S.-I. Itoh, K. Itoh, and T. S. Hahm, Plasma Phys. Controlled Fusion **47**, R35 (2005).